Visualizing Bulk-to-Surface Carrier Diffusion via Band-bending of Solar Cell Materials by 4D Electron Microscopy at Low Applied Potential

Ahmed M. El-Zohry*[a,b], Basamat S. Shaheen[a], Thomas G. Allen[a], Michele De Bastiani[a], Mohamed N Hedhili[c], Stefaan De Wolf[a], Boon S. Ooi[d], and Omar F. Mohammed[a]*

[a] Physical Sciences and Engineering Division, King Abdullah University of Science and Technology (KAUST), Thuwal 23955-6900, KSA.
[b] Department of Physics - AlbaNova Universitetscentrum, Stockholm University, SE-10691 Stockholm, Sweden.
[c] King Abdullah University of Science and Technology (KAUST), Core Labs, Thuwal 23955-6900, KSA.
[d] Photonics Laboratory, King Abdullah University of Science and Technology (KAUST), Thuwal 23955-6900, KSA.
*amfzohry@yahoo.com, omar.abdelsaboor@kaust.edu.sa.

Abstract

Utilizing four-dimensional scanning ultrafast electron microscopy (4D-SUEM) is a powerful tool to monitor charge dynamics at material surfaces and interfaces especially for the application in renewable energy field. Herein, we uncover unique physical features for 4D-SUEM upon reducing the acceleration of probed primary electrons to 1 keV, for wide range of materials including various single crystals, thin films and quantum dots upon the presence of oxidized and neat surfaces. Working at 1 keV helps to uncover the migration of photogenerated carriers originating from both sub-surface and bulk layers, under the influence of the carriers scattering and the band-bending phenomena. This approach provides a new avenue for the spatial and temporal access to the surface exclusive dynamics in renewable energy materials to unlock their interfacial behaviors at the nanoscale level.

TOC Graphic

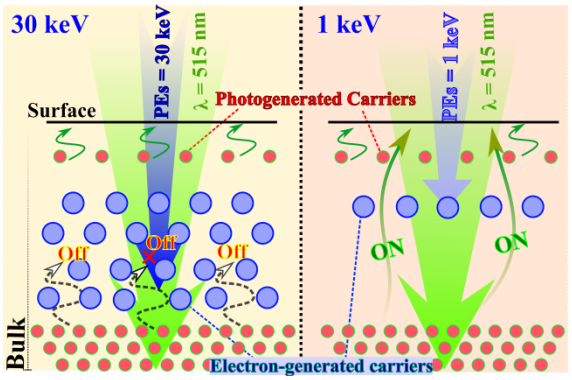

Introduction

Understanding charge carrier transport in crystalline and amorphous semiconductors is a critical step to achieving high performances in devices such as thin-film transistors, light-emitting diodes, and solar cells.[1] This transport directly depends on the carrier (*i.e.* electron or hole) diffusivity, controlling the efficiency in the aforementioned applications.[2] Generally, when electrons in a semiconductor have excess energy, they exhibit mobility through various electronic states distributed through the entire specimen. This mobility can be determined by measuring either carrier mobility or carrier diffusivity. In the presence of an applied electric field on the specimen, the carrier mobility/diffusivity depends on the excess energy of the carrier and the mean free paths for carriers between different scattering occasions, in which the higher carrier mobility is assigned to longer mean free path.[1] The direct relation between carrier mobility (μ) and its diffusion coefficient (D) at an ambient temperature (T) is expressed in the Einstein equation: $D = \frac{kT}{q}\mu$, in which q is the unit charge and k is the Boltzmann constant.[2] Various techniques are routinely used to determine carrier mobility and carrier diffusion; however, most of these techniques present some drawbacks, such as poor repeatability, low accuracy, absence of high-time resolution, and more importantly lack of surface-sensitivity. [1] Even though there are some time-resolved techniques used to determine the carrier mobility of a specific material, they require additional processing for sample preparation, such as the deposition of electron/hole transporting materials, which, in turn, may undesirably affect the trap-state density and surface morphology of the targeted material.

Four-dimensional scanning ultrafast electron microscopy (4D-SUEM) has recently emerged as a unique tool to study charge dynamics in real-time at material surfaces of a variety of semiconductor materials, such as CIGSe [3], InGaN [4-6], GaAs [7], amorphous Si [8], CdSe [9], CdTe[10], and p-n junctions.[11] In this experiment (see **Scheme 1**, we excite the material by a laser pulse centered at 515 nm, and the surface changes are probed by pulses of primary electrons (PEs) with certain acceleration voltages. [4, 12-15] These PEs generate timely secondary electrons (SEs) from the surface of the specimen that are detected by a positively biased Everhart-Thornley detector, thus reflecting the charge carrier dynamics at the excited state of the material surfaces.[13] Commonly, high applied voltage for primary electrons was set to be 30 keV for 4D-SUEM measurements, to achieve high resolution images for the SEs dynamics.[3, 5, 8, 10, 14, 16-18] However, various materials can be quickly degraded under such high applied voltages affecting the output results.[19] Thus, working at lower

applied voltages is recommended to detect more repeatable measurements. Utilizing 1 keV for the primary electrons could reveal the importance of such voltage to differentiate between oxidized and neat surfaces for various materials, and illustrated that dark images observed in 4D-SUEM can be attributed to the presence of oxidized surfaces. However, all the resulted data show slow rising components that vary from material to another whatever the presence of oxidized surfaces or not.[19] In this work, we try to focus on understanding the nature of these rising components associated with the 4D-SUEM measurements at low applied voltages. We could model the detected slow rising dynamics to the migration of photo charged carriers generated by the penetrating light, and could modulate these slow dynamics by changing the applied voltages of the primary electrons. Thus, herein we show that the usage of a low applied voltage of 1 keV can also directly map and control the charge carrier diffusion process from deep layers at "ca. 10-100s of nanometers" to surface layers for various semiconductor single crystals. Under the 1 keV working condition, the light penetration is deeper than the primary electron penetration, such as in the CdTe single crystal, allowing for, the monitoring of the diffusion of photogenerated charges (PG) formed at the material bulk to the top surface; see **Scheme 1** These surfaces are easily oxidized and could be etched by several methods, which dramatically affect the nature of the observed signals in the 4D-SUEM measurements at 1 keV, revealing the interplay between light and electron penetration depth affects the observed charge dynamics on material surfaces at the nanometer scale. We also studied the influence of the surface oxidation on the surface charge dynamics for various materials, in which band-bending can influence the carrier mobility towards the material surfaces.

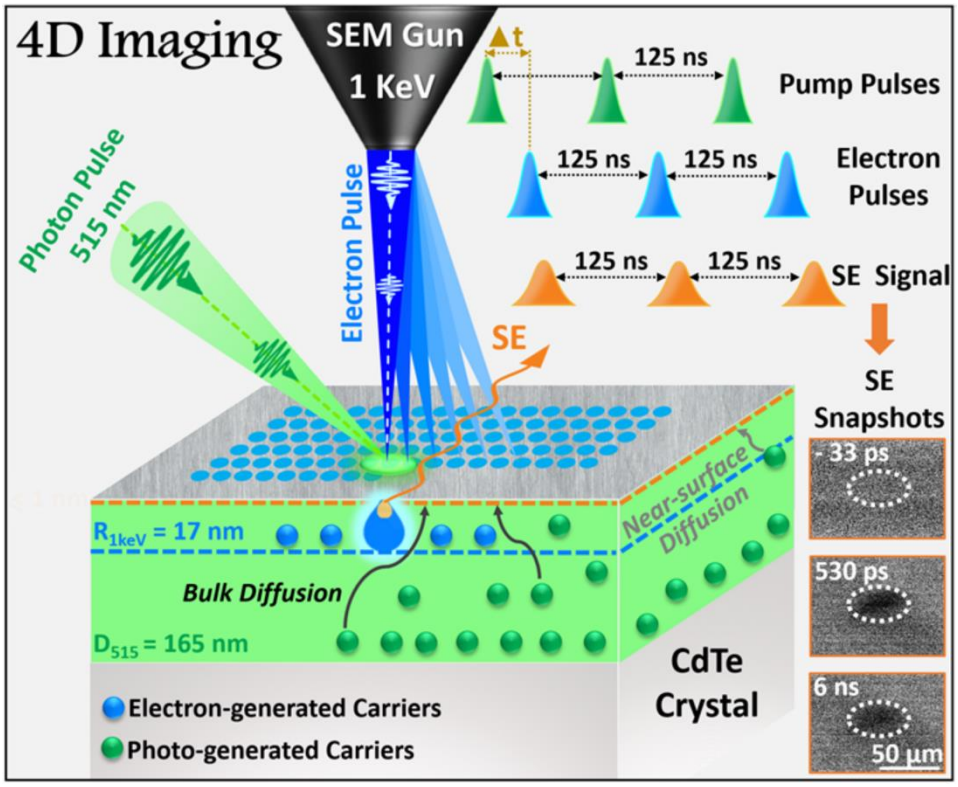

Scheme 1: Schematic representation of four-dimensional scanning ultrafast electron microscopy (4D-SUEM) at 1 keV working condition using an excitation source of 515 nm and a repetition rate of 8 MHz. Using the CdTe single crystal as an example, the 515 nm photon pulse can penetrate ca. 165 nm, while the primary electrons can only penetrate ca. 17 nm, see the main text. The resulting secondary electron signal is generated from the top surface layer of ca. 1 nm, producing dynamic black contrast images due to energy loss mechanisms and surface oxidation; see the main text for more information.

Results and Discussion

Origin of Slow Growing Dynamics at Low Applied Voltages

Figure 1 shows the static and time-resolved secondary electron images at different time delays for the various as-received materials investigated (p-doped CdTe, p-doped CdZnTe, and n-doped Si) at a low applied voltage of 1 keV. These dark contracts were attributed to the presence of oxidized layers as shown previously by XPS measurements (Figure S1-S3).[19] Also, as can be seen for these materials and for others measured at 1 keV, the type of the semiconductor p or n as well as the chemical composition does not provide variation in the type of image contrasts.

Upon extracting and fitting kinetic traces from all these materials measured, slow rising components are always present, followed by various decay components which are attributed to

charge recombination processes.[10, 16, 19] For instance, the dark contrast for CdTe (110), can be fitted by two time components for the best fit (see **Figure 2** and Table 1). These lifetimes include one rise time component of 355 ps and one long-decay component with nanosecond lifetime, as shown in Table 1. Similar observations are also shown for other crystals; see Table 1 and **Figure 1**. Although these rise time components are similar for CdTe single crystals, single crystal Si (100) textured wafers showed a much faster rising component of 110 ps (see **Figure 2**). Interestingly, all of these kinetic traces display slow growing components, which were not observed previously for 4D-SUEM studies at the higher applied voltage of 30 keV with the same 515 nm excitation source.[4, 9, 12-15, 17]

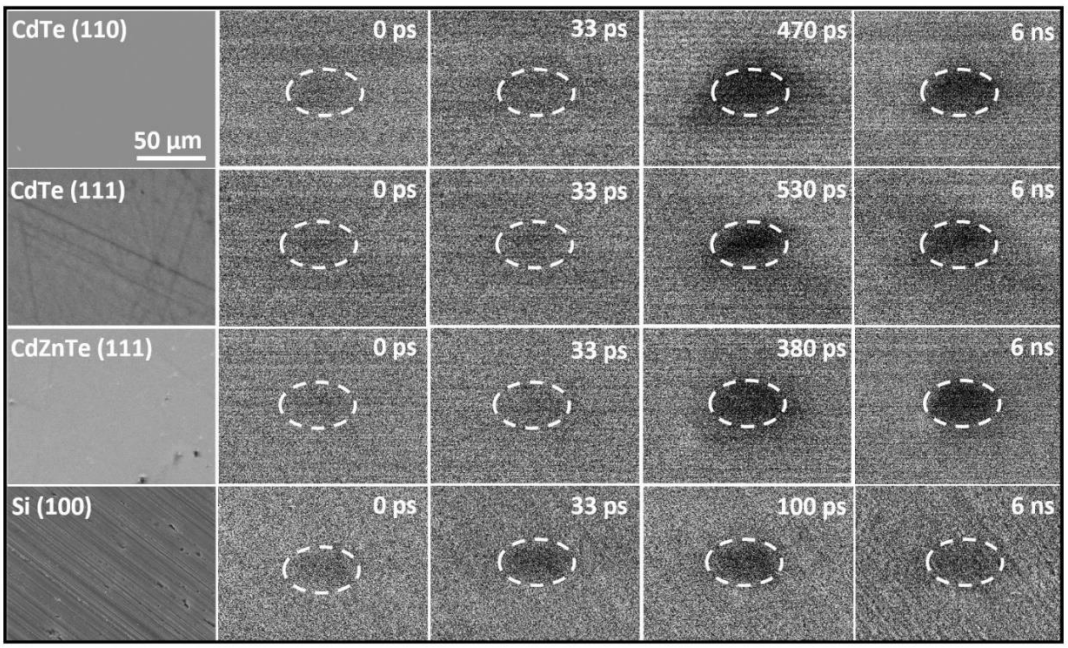

Figure 1: Static SEM images for p-CdTe (110), p-CdTe (111), p-CdZnTe (111), and n-Si (100) surfaces taken by thermal electrons from top to bottom. Different SE images are shown for material surfaces at positive time delays starting from time zero to ca. 6 ns, with shaded areas for the laser footprint, showing the progress of the charge carrier dynamics within each material.

Number of few parameters is needed to be figured out to know the origin of such slow rising components in the time resolved SEs data. To investigate the effect for the number of incident electrons, the CdSe thin film was examined for such experiment. **Figure 3A** shows that the slow-rising component is independent on the number of probed electrons at such low applied voltage used (30 and 100 pico-ambers). This indicates that such slow rising component is not originated from the number of incident primary electrons rather than the electron's energy.

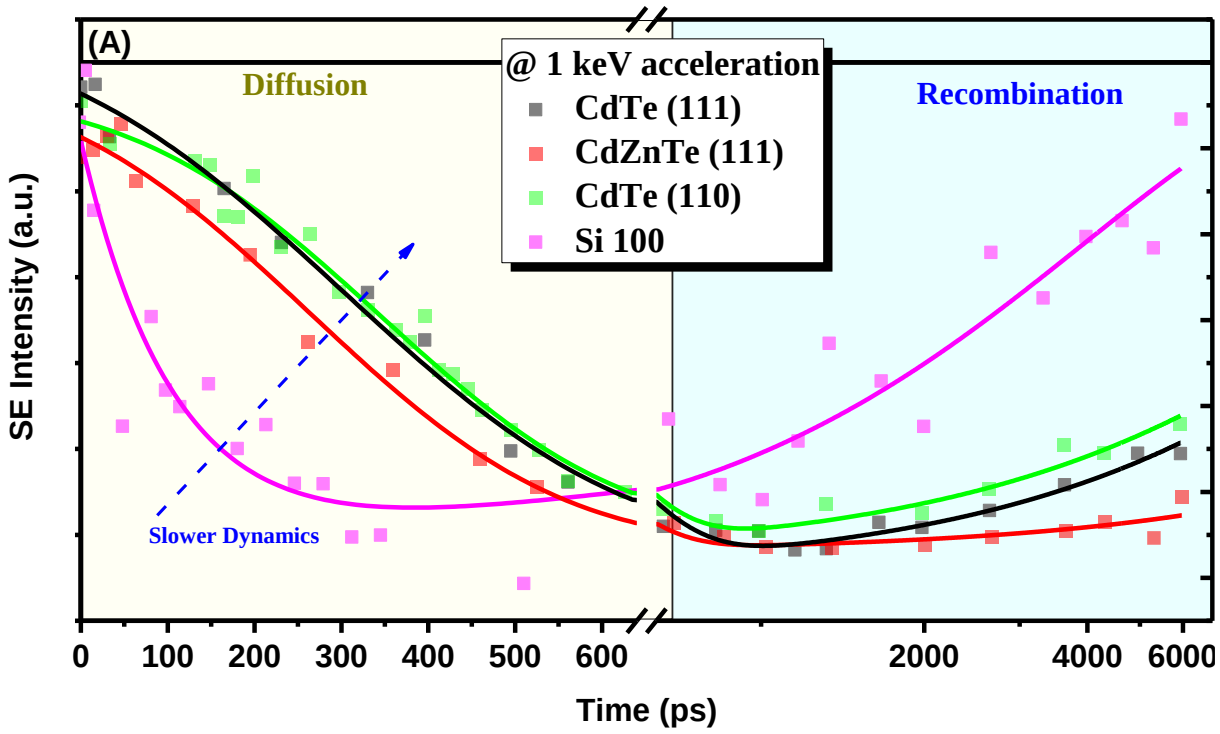

Figure 2: (A) Normalized kinetic traces extracted within the shaded area in **Figure 1**, representing the charge carrier dynamics at Si (100), CdTe (110), CdTe (111), and CdZnTe (111) single crystal surfaces, with shaded areas for charge carrier diffusion (yellow) and charge carrier recombination (cyan) processes.

Table 1**:** Fitting parameters required for fitting the kinetic traces extracted for various materials as listed below. Lifetimes are shown in ps and ns; amplitudes are shown in % between parentheses.

Sample	τ^{diff} (ps)	τ^{1}_{decay} (A_1%)	τ^{2}_{decay} (A_2%)
Si (100)	110±25	4.7±1.1 ns (100)	------
CdTe (110)	355±16		Long (100)
CdTe (111)	305±13		Long (100)
CdZnTe (111)	260±12	---	Long (100)

Another possibility for the slow rising component can be originated from the wide pulse utilized for the time resolved measurements. Upon reducing the energy of probed electrons at 1 keV in each packet, one expects to observe a smaller time resolution, in which the electrical charge is proportional to the applied voltage, as shown in the capacitance relationship[20], an electron pulse

width of 30 fs has been achieved at 0.4 keV.[21] Also, the temporal resolution is mainly controlled by the broadness of the laser pulses used, which was about ~1.2 ps.[22] It should be pointed out that a correlation has been found between the low number of probed electrons and narrowing of the temporal resolution at 30 keV due to Coulomb's repulsion force, in which the temporal resolution was in the range of 0.65 to 3.2 ps.[14] In this case, the presence of slow-rising components at 1 keV of ca. two orders of magnitude higher than FWHM in the case of 30 keV, and cannot be justified by an increase in the temporal resolution at lower applied voltages. However, to characterize the temporal resolution and pulse broadening at 1 keV, we acquired images with high integration time and small time steps (ps) for the CdSe thin film, and FWHM of ca. 2.0 ± 0.9 ps was obtained in addition to the slow rising component; see **Figure 3B**. It is worth mentioning, that the CdSe film shows low amount of oxidation at the Se atom[23] as reveled by the XPS measurement (see Figure S4), and thus the observed surface dynamics from the 4D-SUEM were bright spots with a positive contrast as shown in the inset of **Figure 1**B.

To further scrutinize and verify the effect of applied voltage on the observed rising time components, the Si (100) wafer has been measured at a higher applied voltage of 2 keV, and a slow rise component is also detected, however with a faster rising time component of ca. 57 ps; see **Figure 3C**. Moreover, upon measuring the Si (100) at 30 keV, the fast rise component was fitted to 7.5 ps (This fast rising component is expected to be merged with the pulse width of the laser pulse). These results indicate that a relationship is present between such slow rise components and the applied voltage used for primary electrons. Thus, we assigned these slow rise components observed at 1, 2, 30 keVs for the charge carrier diffusion to the penetration depths of probe pulses of PEs at various applied voltages into these materials, as illustrated below in detail.

To gain more physical insights into the diffusion process from the bulk to the surface, we first calculated the penetration depth of the 515 nm pump-excitation pulses. The light penetration depth in any material relies on the inverse of its absorption coefficient (α). Using reference values of absorption coefficients, the light penetration depths are found to vary from 165 nm in CdTe samples to 1330 nm for Si samples, as shown in **Table 2**. Conventionally, it is known that when light passes through an absorbing medium, creates high density of photogenerated carriers near to the incident surface, and this density is exponentially decaying towards the entire specimen; see **Figure 4** and **Table 2**. According to this picture, the photogenerated carriers diffuse only towards

the bulk due to concentration gradient present. By using the penetration depth of the excitation light and the observed rise time component form the 4D-SUEM measurements for each material, we could calculate the diffusion coefficient (D) of each material using the following equation: $D = (3\alpha^2\tau^{diff})^{-1}$.[2, 24]

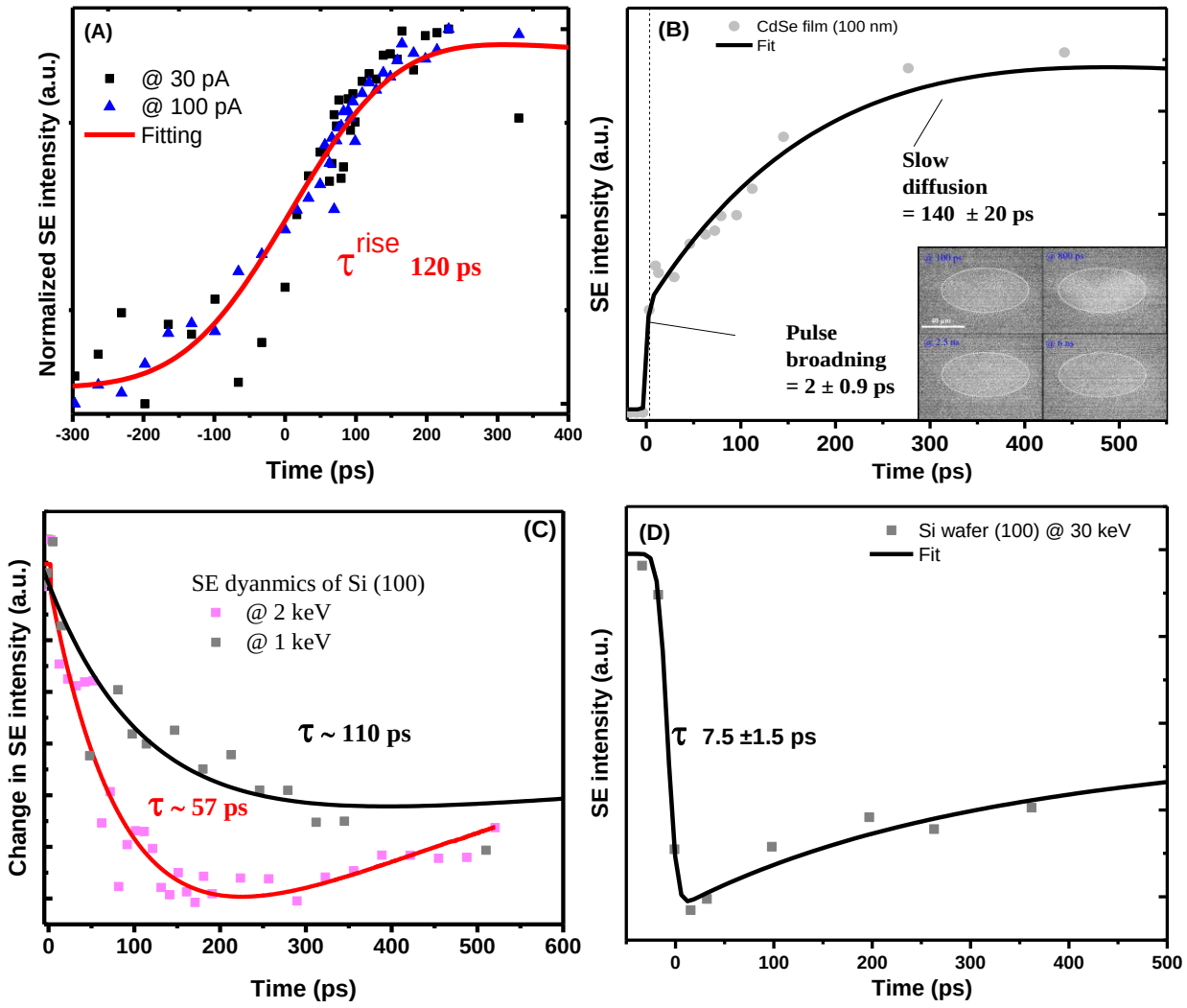

Figure 3: (A) Comparison of kinetic traces of SE signal at 1 keV for a thin film of CdSe (100 nm) at different currents of 30 and 100 pA, with a fitting rise time component of 120 ps. (B) Comparison between normalized kinetic traces of SE dynamics for Si (100) at 1 and 2 keV, showing exponential fitting for the rising components of 110 and 57 ps, respectively. (C) Extracted kinetic trace for 100 nm CdSe thin film with small time steps to measure the FWHM estimated to be within 2 ps and followed by a slow rise. (D) Extracted inverted kinetic trace for the SE intensity of Si wafer (100) at an excitation wavelength of 515 nm and using probed electrons at an applied voltage of 30 keV.

Table 3 shows a comparison of calculated diffusion coefficient values with the literature ones for the same materials. The range of calculated diffusion coefficient values fits quite well with the reported ones after taking into account the range of absorption coefficients used and the noises present in the extracted kinetic traces. Thus, under the 1 keV working conditions, the slow rise of detected SEs could be attributed to the diffusion of photogenerated charges produced by the photon excitation far from the bulk to the top few nanometers of the surface.

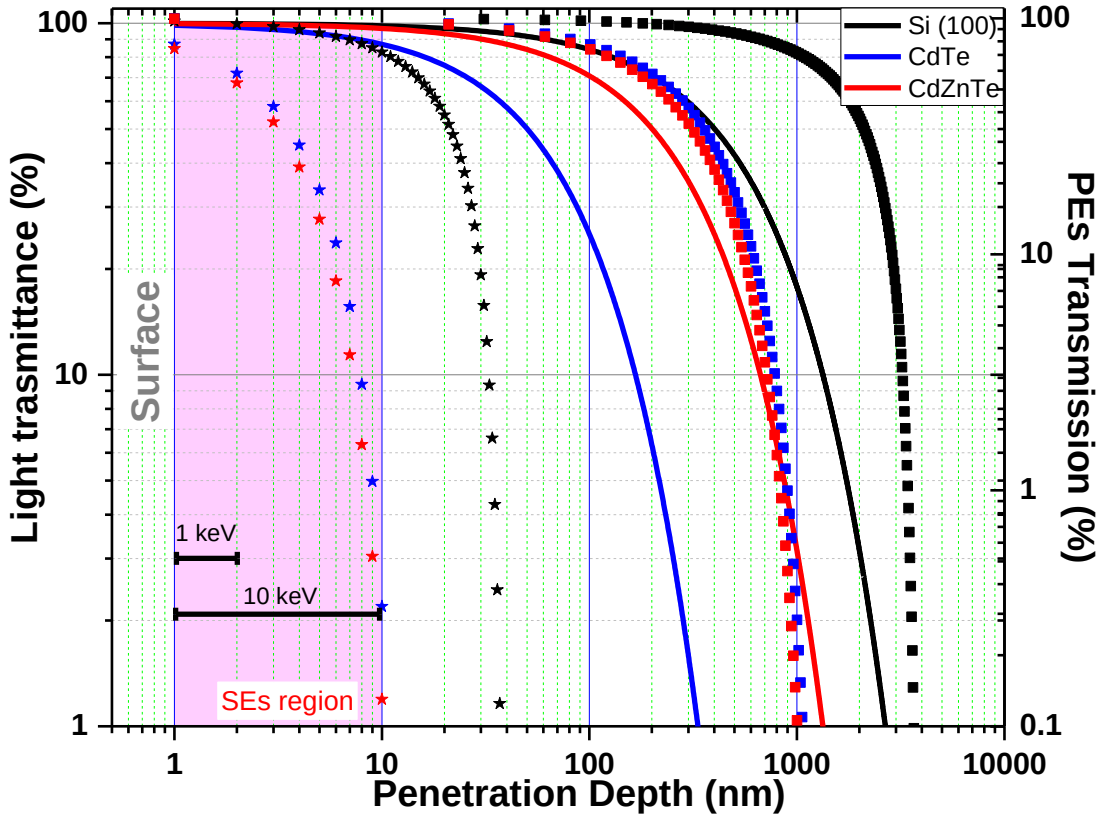

Figure 4: Light penetration depth for investigated materials, Si, CdTe, and CdZnTe, at the wavelength of 515 nm (solid lines of different indicated colors). The penetration depths of primary electrons are shown at different applied voltages of 1 keV (green lines with circles of different colors for each material) and 30 keV (square points of different colors): black (Si), blue (CdTe), and red (CdZnTe). The region of detection of the secondary electrons is shown in pink, near to the material surface. The light penetration depth is calculated using the transmittance relationship ($T = exp(-2.3l\alpha)$) for the investigated materials. More information is presented in the text.

Table 2: Values of primary electron penetration depth at 1 and 30 keV in the investigated materials, along with their densities. The light penetration depth at 515 nm is shown for each material.

Sample	Density (10^6 .µg. cm^{-3})	R^{1keV}(nm)	R^{30keV}(nm)	light penetration depth at $\lambda \approx 515$ nm (nm)
Si	2.33	43	4234	1330
CdTe	5.85	17	1686	165
CdZnTe	5.8	17.2	1700	660

Although the diffusion process of charges from bulk to surface fits the data quite well, this could not explain the absence of such a process in previous 4D-SUEM measurements using the high applied voltage of 30 keV or the change of lifetime components of this process upon using 2 keV; see **Figure 3**. Nevertheless, working with different voltages significantly affects the penetration depth of the primary electron beam. More specifically, the penetration depth of pulsed-primary electrons is limited by the electron energy and the inelastic scattering process with the atomic electrons, as well as by deflection by nuclear collisions.[25] The maximum penetration depth (*R*) for a material of density (ρ) can be estimated at working applied voltage (*E*) through the following equation: $R = aE^{1.35}\rho^{-1}$, in which a is a constant of 10 µg.cm^{-2}.[26] Due to multiple collisions processes for PEs within the target, the transmission of PEs inside the material is controlled by an exponential equation, as shown in Lenard's equation.[25]

$$T_{PEs} = \exp\left(-\frac{0.187Z^{0.666}\times depth}{(R-depth)}\right)$$, where Z is the target atomic number

Table 3: Comparison of measured diffusion constants according to measured diffusion lifetimes obtained via 4D-SUEM versus literature values of diffusion coefficients from other techniques.

Sample	Absorption cross section (α, cm^{-1})[Ref.]	Diffusion time (τ^{diff})	Diffusion coefficient from bulk to surface (D, $cm^2.s^{-1}$)	Reported diffusion coefficient ($cm^2.s^{-1}$)[Ref.]
Si (100)	(ca. $6\text{-}9\times10^3$)[27-29]	110 ps	ca. 84-37	36-10[24, 30-31]
CdTe (110)	(ca. $2\text{-}10\times10^4$)[28-29, 32-33]	355 ps	ca. 2.2-0.09	3.0[34]
CdTe (111)	(ca. $2\text{-}10\times10^4$)[28-29, 32-33]	300 ps	ca. 2.8-0.1	3.0[34]
CdZnTe(111)	(ca. $1\text{-}2\times10^4$)[35]	260 ps	ca. 12.8-3.2	8.1-1.7[34]

Figure 4 and **Table 2** show the penetration depth of primary electrons in Si and CdTe materials at different applied voltages of 1 and 30 keV according to Lenard's equation. For example, the maximum penetration depths of primary electrons at 1 keV range from ca. 17 to 43 nm for CdTe and Si, respectively (see

Table 3 shows a comparison of calculated diffusion coefficient values with the literature ones for the same materials. The range of calculated diffusion coefficient values fits quite well with the reported ones after taking into account the range of absorption coefficients used and the noises present in the extracted kinetic traces. Thus, under the 1 keV working conditions, the slow rise of detected SEs could be attributed to the diffusion of photogenerated charges produced by the photon excitation far from the bulk to the top few nanometers of the surface.

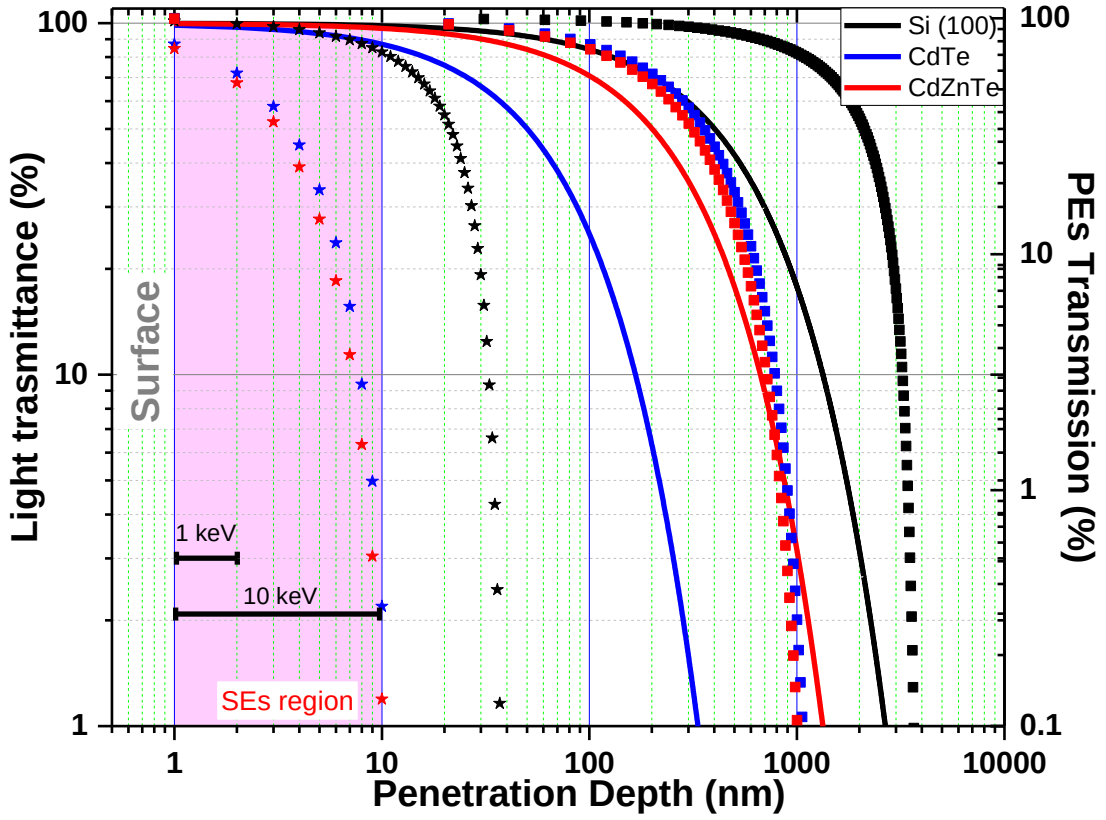

Figure 4: Light penetration depth for investigated materials, Si, CdTe, and CdZnTe, at the wavelength of 515 nm (solid lines of different indicated colors). The penetration depths of primary electrons are shown at different applied voltages of 1 keV (green lines with circles of different colors for each material) and 30 keV (square points of different colors): black (Si), blue (CdTe), and red (CdZnTe). The region of detection of the secondary electrons is shown in pink, near to the material surface. The light penetration depth is calculated using the transmittance relationship ($T = exp(-2.3l\alpha)$) for the investigated materials. More information is presented in the text.

Table 2). In contrast, these values are two orders of magnitude higher at 30 keV (see **Table 2**

Table 3 shows a comparison of calculated diffusion coefficient values with the literature ones for the same materials. The range of calculated diffusion coefficient values fits quite well with the reported ones after taking into account the range of absorption coefficients used and the noises present in the extracted kinetic traces. Thus, under the 1 keV working conditions, the slow rise of

detected SEs could be attributed to the diffusion of photogenerated charges produced by the photon excitation far from the bulk to the top few nanometers of the surface.

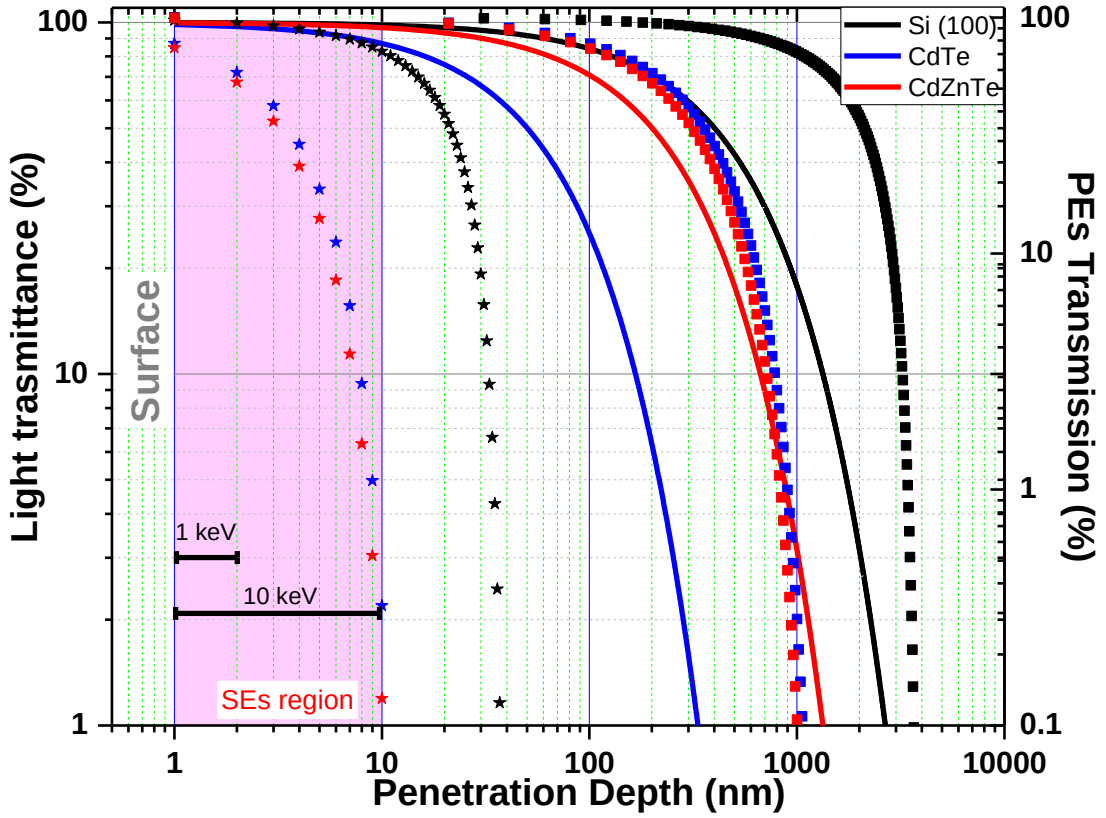

Figure 4: Light penetration depth for investigated materials, Si, CdTe, and CdZnTe, at the wavelength of 515 nm (solid lines of different indicated colors). The penetration depths of primary electrons are shown at different applied voltages of 1 keV (green lines with circles of different colors for each material) and 30 keV (square points of different colors): black (Si), blue (CdTe), and red (CdZnTe). The region of detection of the secondary electrons is shown in pink, near to the material surface. The light penetration depth is calculated using the transmittance relationship ($T = exp(-2.3l\alpha)$) for the investigated materials. More information is presented in the text.

Table 2). Upon comparing these values with the light penetration depth, one finds that the light penetration depth is almost one order of magnitude higher for CdTe samples and 30 times higher

for the Si samples in comparison with primary electron penetration at 1 keV (see **Table 2**). On the other hand, at 30 keV, the light penetration depths are much smaller than the electron penetration depth (see **Table 2**). These regions of deep photogenerated carriers far from the top surface are overlapped solely with the penetration depth of the PEs at 30 keV (see **Figure 4**). Thus, these calculations show that the photogenerated charge carriers within the material bulk populated by the photon excitation can diffuse in many directions, including towards the material surface. With high voltage 30 keV electrons, the highly penetrated primary electrons can scatter with the deeply formed photogenerated carriers within the bulk, thus suppressing their mobility towards the surface through inelastic carrier-carrier scattering processes. In this case, the detected dynamic SE signals at such high voltages are produced mainly from the photogenerated carriers near to the material's surface when the absorbed light intensity approaches 1-1/e. This can be easily transferred into nanometer depths of ca. 30 nm, 125 nm, and 250 nm for CdTe, CdZnTe, and Si, respectively. By using the diffusion coefficient values from **Table 3**, we can theoretically calculate the appearance "rise" component for the SE signals at 30 keV, when the majority of bulk carriers are inhibited. Relying on the reported diffusion values, the rise lifetimes can be as follows 3 ps ($D \approx 3$ cm^2.s^{-1}), 8.7 ps ($D \approx 6$ cm^2.s^{-1}), and 5.8 ps ($D \approx 36$ cm^2.s^{-1}) for CdTe, CdZnTe, and Si, respectively. These rise lifetime components simply fall in the same range reported previously for the broadening of the 30 keV-probed electron wave packets.[4, 12-15]

It should be noted that, due to the low primary electron penetration depth of 1 keV electrons, the carrier inelastic scattering is much less compared to 30 keV electrons, thus facilitating the observation of overwhelming photogenerated carrier diffusion from the material bulks to the surfaces as shown, rather than the photogenerated carriers produced near the surface; see **Figure 3B**. At 2 keV, in which case the $R^{2keV} \approx 110$ nm for Si wafer, the SE signal displays a faster kinetic component (57 ps) due to diffusion of fast carriers nearer to the surface; see **Figure 3A**. The rising time of 57 ps can correspond to a depth of 780 nm for the diffusion of bulk carriers ($D \approx 36$ cm^2.s^{-1}), instead of the 1330 nm depth at 1 keV (**Figure 3**). In addition, upon measuring the same Si wafer under the same working conditions at 30 keV, only a fast rise of 7.5 ±1.5 ps was observed, followed by slow signal decay, which is very close to previous calculations; see **Figure 3D**. This finding is in line with the proposed mechanism that increasing the applied voltage of the PEs will result in penetration more strongly inhibiting the slow diffusing carriers from deep layers via

inelastic scattering processes, thus allowing fast carriers from subsurface layers to reach the surface earlier.

Impact of Oxide Layer on the Observed Dynamics

The above model indicates that, the slow rising components upon working at low applied voltage like 1 keV can be assigned to the migration of photogenerated carriers at the bulk to the surface, which doesn't exclude the migration of photogenerated carriers at the sub-surface levels detected at the 30 keV working conditions. In other words, high applied voltages should be sensitive to the sub-surface layers, and the low applied voltages should be sensitive to both sub-surface and bulk migrations of photogenerated carriers. However, the fast responses from the migration of subsurface photogenerated carriers are not quite well-resolved at the data presented in **Figure 2**.

To seek that fast rising lifetime, several scans were performed for an oxidized PbS quantum dots[36] with small delay time steps around time zero, as PbS illustrated strong dynamical signal under the working conditions giving a high signal to noise ratio, in comparison to other oxidized materials used. **Figure 5A** shows the kinetic trace of PbS extracted from the time-resolved images round time zero. Interestingly, around time zero, weak bright images form the oxidized PbS could be measured, which are quickly converted into dark images that are present in the extracted kinetic trace. The kinetic trace is fitted with two lifetimes; the first one is a fast decay lifetime (15±10 ps), while the second one is a slow growing lifetime 160±30 ps. Recently, at 1 keV working conditions, we assigned the presence of bright images to the absence of oxidation layers and the presence of dark images to the presence of oxidation layers.[19] Thus, the initial fast decays component along the conversion of bright images to dark, detected herein for the oxidized PbS material, can be assigned the ultrafast trapping of photogenerated carriers at the surface, which is followed by slow diffusion from bulk carriers. For further confirmations, CdTe crystals were etched and re-measured by 4DSUEM with small delay steps around time zero. The XPS measurements of the Ar-etched CdZnTe (111) and CdTe (110) show the disappearance of the adsorbed oxygen on surface and the Te-oxides, respectively. The extracted kinetic traces from the 4D-SUEM shows a fast rise components of 2-4 ps followed by slow rises of ca. 430-500 ps, then a long lived lifetime components are observed for the two samples; see **Figure 5 B-C**. Similarly, the HF-etching of the Si sample shows disappearance of the Si-oxide peaks, and the presence of bright contrasts, with

fast rise component of 5 ps and a slow component of 330 ps, followed by a long lived species on surfaces. Overall, whatever dark or bright contrasts are observed in the above dynamics, the slow rising components, in the orders of tens of ps, is present in both oxidized and fresh etched samples at 1 keV, and can be easily separated from the fast rising component due to migration of subsurface carriers. Accordingly, we assign these slow rising components to carriers' diffusion from the materials' bulk to surfaces.

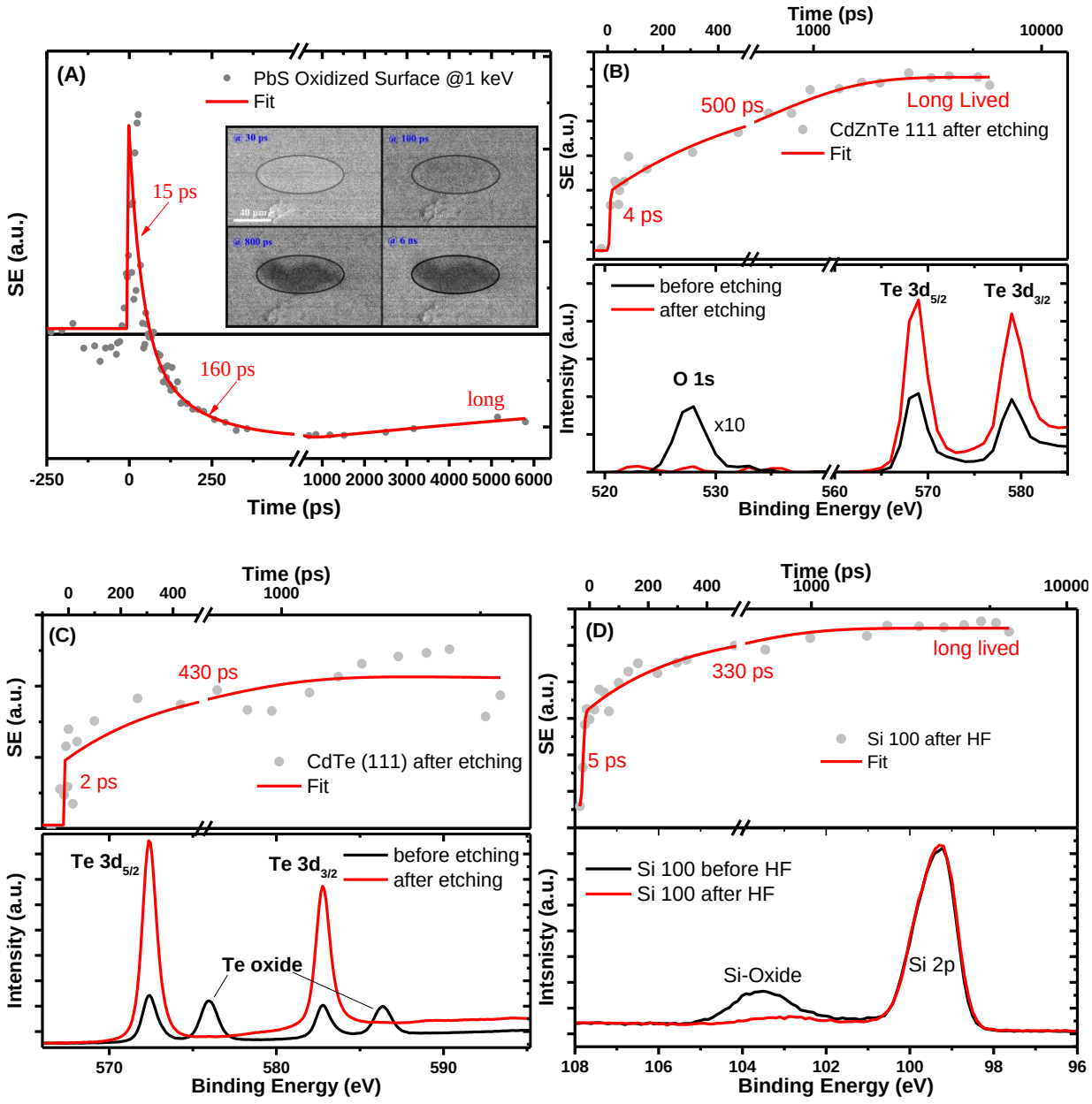

Figure 5: (A) Extracted kinetic trace for PbS oxidized single crystal with small time steps to measure the electron trapping process at oxidized surface with high signal to noise ratio, which is followed by a slow rise of the negative signal. The inset shows some extracted images at various times for the measured signal using 4D-SUEM. (B) Extracted kinetic trace for the CdZnTe single crystal after Ar etching in the XPS chamber. The XPS data for effect of etching is shown below, illustrating the disappearance of adsorbed oxygen. (C) Extracted kinetic trace for the CdTe single crystal after Ar etching in the XPS chamber. The XPS data for effect of etching is shown below, illustrating the disappearance of Te-oxide peaks. (D) Extracted kinetic trace from the etched Si (100) surface after HF treatment (top). Comparison of XPS spectra for treated and untreated Si sample, showing the disappearance of Si-Oxide peak upon etching. See main text for more information.

Band Bending Effect

From the XPS data presented earlier for several materials, the investigated surfaces herein are already oxidized physically and chemically by oxygen and carbon substances. Upon band-gap excitation with 515 nm, electron-hole pairs will be formed at the oxidized material surface, in which the electrons in the conduction band have higher probability to produce SEs, giving a bright contrast around time zero at the 4D-SUEM images as shown in **Figure 5**. The presence of oxidized species at surfaces will apparently cause two effects: (1) form trapping-surface states, which in turn will induce formation band-bending at the materials' surfaces, [37-38] see **Scheme 2**. (2) These oxidized species act as electron's sink, in which the photogenerated carriers (electrons) will be quickly trapped, few ps, to those oxidized surface species. Thus, upon photoexcitation, fraction of the surface electrons will be quickly trapped into the oxidized layers, which is shown in the case of oxidized PbS at early time (see **Figure 5A**). The rest of the surface electrons, if present, will migrate into the material bulk until thermal equilibrium is achieved forming a depletion layer at the surface as shown in A. While the photogenerated holes will migrate, depending on the hole-mobility, to the material surface under the same effect, causing to the appearance of dark images for the oxidized layers and the appearance of slow growing negative components. Apparently, the detection of the brightness at early times for oxidized materials depends on the level of the oxidation and the rate for electron trapping for each particular material. Moreover, the detection of the fast response from holes located near to the surface may no easy to detect due to the overlap of the negative signal from holes with the positive signal from electrons near to the surface.

Upon cleaning or etching the semiconductor surfaces chemically or physically, all the detected signals from 4D-SUEM at 1 keV converted into positive ones "bright contrast", mainly due the

population of electrons at the material surfaces and the absence of trapping species.[19] However, slow growing positive components are also found on the cleaned surfaces. Knowing that cleaned surfaces means that the surface atoms are under-coordinated condition and not under thermal equilibrium as shown previously. [39-40] Thus, the migration of electrons populated form the bulk to the surface can be understood upon the presence of accumulation layer at the surface, causing the downward band-bending at the surface layers; see **Scheme 2B**. However, the slow rise measured lifetimes especially for Si (100), CdTe (111) and CdZnTe (111) are longer than corresponding ones before etching with lower amplitudes; see **Figure 5**. This can be understood through two scenarios; the first is that electrons mobility is lower than hole mobility that is not likely, or that the width of the accumulation layer is smaller compared to the depletion layer associated with trapping species present before etching.[37] Apparently, the width of accumulation layer is smaller than corresponding depletion layers, leading to small potential difference upon cleaning, and making the electrons mobility towards the surface have smaller mobility than holes; see **Scheme 2**. Thus, under the 1 keV working condition, the slow rise of detected SEs "dark or bright" could be attributed to the diffusion of photogenerated charges "holes or electrons" produced by the photon excitation from the bulk to the top few nanometers of the surface under the band-bending effect created by either the formation of depletion or accumulation layers. Also, due to the absence of electron trapping process at cleaned surfaces, it was also possible to detect the fast response of electrons near to the surface at early time scale, few picoseconds.

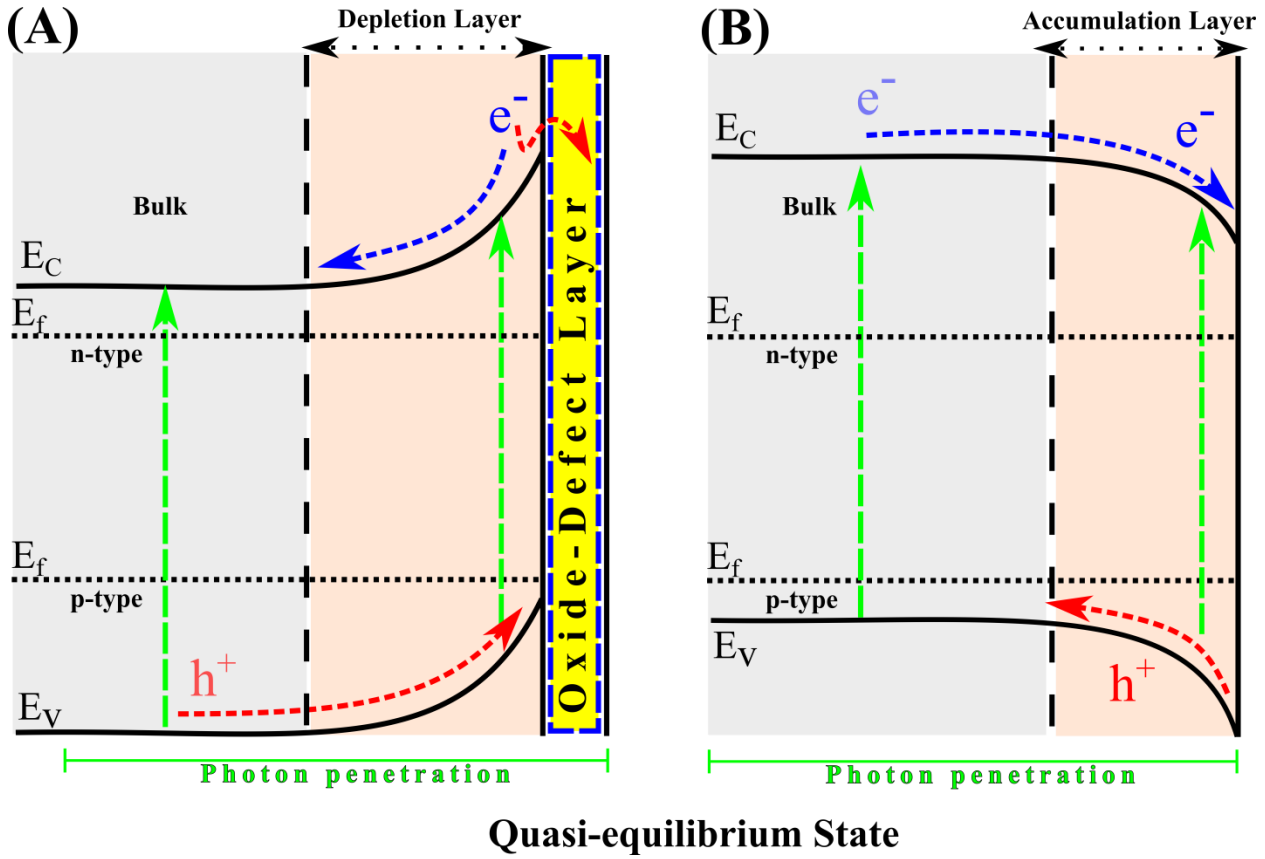

Scheme 2: Simple representation for the observed dynamics in semiconductors using low voltage of 1 keV of 4D-SUEM, after light excitation, in the presence of oxidation layers (A), and after removing the oxidation layers (B). More details are found in the text.

Conclusions

In summary, using 4D electron imaging at low applied voltages for various materials allows for the detecting of: (1) The nature of surface state, whether oxidation layers are present or not. (2) Migration of photogenerated charges from the bulk to the material surface. (3) Study the band-bending effect along with the possible estimation for depletion or accumulation layers. Herein, we visualized the charge carrier diffusion on the surface of solar cell absorber materials in real space and real time. At high applied voltage of 30 keV, only surface charge-carrier dynamics can be observed, as the charge carrier diffusion from the bulk to the top surface is suppressed due to strong electron-electron inelastic scattering processes between the highly penetrated primary electrons and the photogenerated charges located within the material bulk. On the other hand, the reduction of the energy/speed of the primary electrons to 1.0 keV significantly minimizes the electron-electron inelastic scattering processes at the bulk, thus making it possible to access and visualize

carrier diffusion from the bulk to the top surface of the photoactive materials. These new findings provide the foundation for potential applications of 4D-SUEM to access the fundamental dynamic processes at the nanometer scale on the surface of solar cell materials; such information cannot be acquired by any other time-resolved technique.

Acknowledgement

The research reported in this publication was supported by funding from King Abdullah University of Science and Technology (KAUST).

References

1 . Marshall, J. M., Carrier Diffusion in Amorphous-Semiconductors. *Rep Prog Phys* **1983**, *46*, 1235-1282.
2 . Pierret, R. F.; Neudeck, G. W., *Advanced Semiconductor Fundamentals*; Addison-Wesley Reading, MA, 1987; Vol. 6.
3 . Bose, R.; Bera, A.; Parida, M. R.; Adhikari, A.; Shaheen, B. S.; Alarousu, E.; Sun, J. Y.; Wu, T.; Bakr, O. M.; Mohammed, O. F., Real-Space Mapping of Surface Trap States in Cigse Nanocrystals Using 4d Electron Microscopy. *Nano Lett* **2016**, *16*, 4417-4423.
4 . Sun, J. Y.; Adhikari, A.; Shaheen, B. S.; Yang, H. Z.; Mohammed, O. F., Mapping Carrier Dynamics on Material Surfaces in Space and Time Using Scanning Ultrafast Electron Microscopy. *J. Phys. Chem. Lett.* **2016**, *7*, 985-994.
5 . Bose, R., et al., Imaging Localized Energy States in Silicon-Doped Ingan Nanowires Using 4d Electron Microscopy. *ACS Energy Lett.* **2018**, *3*, 476-481.
6 . Bose, R., et al., Real-Space Visualization of Energy Loss and Carrier Diffusion in a Semiconductor Nanowire Array Using 4d Electron Microscopy. *Adv. Mater.* **2016**, *28*, 5106-5111.
7 . Chen, B.; Fu, X. W.; Tang, J.; Lysevych, M.; Tan, H. H.; Jagadish, C.; Zewail, A. H., Dynamics and Control of Gold-Encapped Gallium Arsenide Nanowires Imaged by 4d Electron Microscopy. *PNAS* **2017**, *114*, 12876-12881.
8 . Liao, B.; Najafi, E.; Li, H.; Minnich, A. J.; Zewail, A. H., Photo-Excited Hot Carrier Dynamics in Hydrogenated Amorphous Silicon Imaged by 4d Electron Microscopy. *Nat. Nanotec.* **2017**, *12*, 871-876.
9 . Shaheen, B. S.; Sun, J. Y.; Yang, D. S.; Mohammed, O. F., Spatiotemporal Observation of Electron-Impact Dynamics in Photovoltaic Materials Using 4d Electron Microscopy. *J. Phys. Chem. Lett.* **2017**, *8*, 2455-2462.
10 . El-Zohry, A. M.; Shaheen, B. S.; Burlakov, V. M.; Yin, J.; Hedhili, M. N.; Shikin, S.; Ooi, B.; Bakr, O. M.; Mohammed, O. F., Extraordinary Carrier Diffusion on Cdte Surfaces Uncovered by 4d Electron Microscopy. *Chem* **2019**, *5*, 497-499.
11 . Najafi, E.; Scarborough, T. D.; Tang, J.; Zewail, A., Four-Dimensional Imaging of Carrier Interface Dynamics in P-N Junctions. *Science* **2015**, *347*, 164-167.

12 . Sun, J. Y.; Melnikov, V. A.; Khan, J. I.; Mohammed, O. F., Real-Space Imaging of Carrier Dynamics of Materials Surfaces by Second-Generation Four-Dimensional Scanning Ultrafast Electron Microscopy. *J. Phys. Chem. Lett.* **2015**, *6*, 3884-3890.
13 . Mohammed, O. F.; Yang, D. S.; Pal, S. K.; Zewail, A. H., 4d Scanning Ultrafast Electron Microscopy: Visualization of Materials Surface Dynamics. *J. Am. Chem. Soc.* **2011**, *133*, 7708-7711.
14 . Zewail, A. H., Four-Dimensional Electron Microscopy. *Science* **2010**, *328*, 187-193.
15 . Yang, D. S.; Mohammed, O. F.; Zewail, A. H., Scanning Ultrafast Electron Microscopy. *PNAS* **2010**, *107*, 14993-14998.
16 . Shaheen, B. S.; El-Zohry, A. M.; Yin, J.; De Bastiani, M.; De Wolf, S.; Bakr, O. M.; Mohammed, O. F., Visualization of Charge Carrier Trapping in Silicon at the Atomic Surface Level Using Four-Dimensional Electron Imaging. *JPCL* **2019**, *10*, 1960-1966.
17 . Adhikari, A.; Eliason, J. K.; Sun, J.; Bose, R.; Flannigan, D. J.; Mohammed, O. F., Four-Dimensional Ultrafast Electron Microscopy: Insights into an Emerging Technique. *ACS Appl. Mater. Interfaces* **2017**, *9*, 3-16.
18 . Khan, J. I.; Adhikari, A.; Sun, J. Y.; Priante, D.; Bose, R.; Shaheen, B. S.; Ng, T. K.; Zhao, C.; Bakr, O. M.; Ooi, B. S.; Mohammed, O. F., Enhanced Optoelectronic Performance of a Passivated Nanowire-Based Device: Key Information from Real-Space Imaging Using 4d Electron Microscopy. *Small* **2016**, *12*, 2313-2320.
19 . Shaheen, B. S.; El-Zohry, A. M.; Zhao, J.; Yin, J.; Hedhili, M. N.; Bakr, O. M.; Mohammed, O. F., Real-Space Mapping of Surface-Oxygen Defect States in Photovoltaic Materials Using Low-Voltage Scanning Ultrafast Electron Microscopy. *ACS Appl. Mater. Interfaces* **2020**, *12*, 7760-7767.
20 . Greason, W. D., *Electrostatic Discharge in Electronics*; Research Studies Press, 1992.
21 . Irvine, S. E.; Dechant, A.; Elezzabi, A. Y., Generation of 0.4-Kev Femtosecond Electron Pulses Using Impulsively Excited Surface Plasmons. *Phys. Rev. Lett.* **2004**, *93*.
22 . Li, C.; Mao, S. F.; Ding, Z. J., Time-Dependent Characteristics of Secondary Electron Emission. *J. Appl. Phys.* **2019**, *125*.
23 . Masson, D. P.; Lockwood, D. J.; Graham, M. J., Thermal Oxide on Cdse. *J. Appl. Phys.* **1997**, *82*, 1632-1639.
24 . Brunetti, R.; Jacoboni, C.; Nava, F.; Reggiani, L.; Bosman, G.; Zijlstra, R. J. J., Diffusion-Coefficient of Electrons in Silicon. *J. Appl. Phys.* **1981**, *52*, 6713-6722.
25 . Kanaya, K.; Okayama, S., Penetration and Energy-Loss Theory of Electrons in Solid Targets. *J. Phys. D Appl. Phys.* **1972**, *5*, 43-&.
26 . Egerton, R. F., Physical Principles of Electron Microscopy - an Introduction to Microscopy. In *Physical Principles of Electron Microscopy - an Introduction to Tem, Sem, and Aem*, Springer: 2016; pp 1-195.
27 . Green, M. A.; Keevers, M. J., Optical-Properties of Intrinsic Silicon at 300 K. *Prog. Photovolt.* **1995**, *3*, 189-192.
28 . Jean, J.; Mahony, T. S.; Bozyigit, D.; Sponseller, M.; Holovsky, J.; Bawendi, M. G.; Bulovic, V., Radiative Efficiency Limit with Band Tailing Exceeds 30% for Quantum Dot Solar Cells. *ACS Energy Lett.* **2017**, *2*, 2616-2624.
29 . Mertens, K., *Photovoltaics: Fundamentals, Technology, and Practice*; John Wiley & Sons, 2018.
30 . Najafi, E.; Ivanov, V.; Zewail, A.; Bernardi, M., Super-Diffusion of Excited Carriers in Semiconductors. *Nat. Commun.* **2017**, *8*, 15177.

31 . Li, S. S.; Thurber, W. R., The Dopant Density and Temperature Dependence of Electron Mobility and Resistivity in N-Type Silicon. *Solid-State Electronics* **1977**, *20*, 609-616.
32 . Rakhshani, A. E., Electrodeposited Cdte - Optical Properties. *J. Appl. Phys.* **1997**, *81*, 7988-7993.
33 . Mitchell, K.; Fahrenbruch, A. L.; Bube, R. H., Photovoltaic Determination of Optical-Absorption Coefficient in Cdte. *J. Appl. Phys.* **1977**, *48*, 829-830.
34 . Sudzius, M.; Aleksiejunas, R.; Jarasiunas, K.; Verstraeten, D.; Launay, J. C., Investigation of Nonequilibrium Carrier Transport in Vanadium-Doped Cdte and Cdznte Crystals Using the Time-Resolved Four-Wave Mixing Technique. *Semicond. Sci. Tech.* **2003**, *18*, 367-376.
35 . Lee, D.; Zucker, J. E.; Johnson, A. M.; Feldman, R. D.; Austin, R. F., Room-Temperature Excitonic Saturation in Cdznte/Znte Quantum-Wells. *Appl. Phys. Lett.* **1990**, *57*, 1132-1134.
36 . Malgras, V.; Nattestad, A.; Yamauchi, Y.; Dou, S. X.; Kim, J. H., The Effect of Surface Passivation on the Structure of Sulphur-Rich Pbs Colloidal Quantum Dots for Photovoltaic Application. *Nanoscale* **2015**, *7*, 5706-5711.
37 . Zhang, Z.; Yates, J. T., Band Bending in Semiconductors: Chemical and Physical Consequences at Surfaces and Interfaces. *Chem. Rev.* **2012**, *112*, 5520-5551.
38 . Zangwill, A., *Physics at Surfaces*; Cambridge university press, 1988.
39 . Duke, C. B.; Lubinsky, A. R.; Lee, B. W.; Mark, P., Atomic Geometry of Cleavage Surfaces of Tetrahedrally Coordinated Compound Semiconductors. *Journal of Vacuum Science and Technology* **1976**, *13*, 761-768.
40 . Baraldi, A.; Bianchettin, L.; Vesselli, E.; Gironcoli, S. d.; Lizzit, S.; Petaccia, L.; Zampieri, G.; Comelli, G.; Rosei, R., Highly under-Coordinated Atoms at Rh Surfaces: Interplay of Strain and Coordination Effects on Core Level Shift. *New Journal of Physics* **2007**, *9*, 143-143.